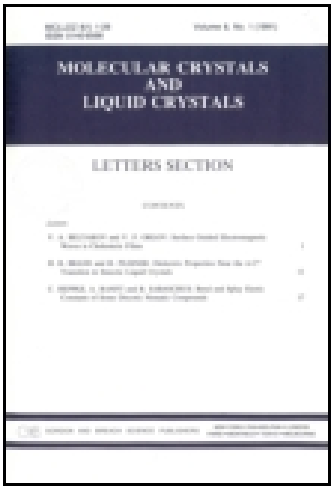

Molecular Crystals and Liquid Crystals
Publication details, including instructions for authors and subscription information:
http://www.tandfonline.com/loi/gmcl20

Thiophene/Phenylene Co-Oligomers as Novel Photovoltaic Materials

Naoki Iwamoto[a], Masashi Nakamura[a], Kenji Ohga[a], Takeshi Yamao[a] & Shu Hotta[a]

[a] Department of Macromolecular Science and Engineering, Kyoto Institute of Technology, Matsugasaki, Sakyo-ku, Kyoto, Japan

Published online: 17 Nov 2014.

To cite this article: Naoki Iwamoto, Masashi Nakamura, Kenji Ohga, Takeshi Yamao & Shu Hotta (2014) Thiophene/Phenylene Co-Oligomers as Novel Photovoltaic Materials, Molecular Crystals and Liquid Crystals, 597:1, 20-28, DOI: 10.1080/15421406.2014.931777

To link to this article: http://dx.doi.org/10.1080/15421406.2014.931777

Mol. Cryst. Liq. Cryst., Vol. 597: pp. 20–28, 2014

ISSN: 1542-1406 print/1563-5287 online
DOI: 10.1080/15421406.2014.931777

Taylor & Francis
Taylor & Francis Group

Thiophene/Phenylene Co-Oligomers as Novel Photovoltaic Materials

NAOKI IWAMOTO, MASASHI NAKAMURA, KENJI OHGA, TAKESHI YAMAO, AND SHU HOTTA*

Department of Macromolecular Science and Engineering, Kyoto Institute of Technology, Matsugasaki, Sakyo-ku, Kyoto, Japan

We applied thiophene/phenylene co-oligomers (TPCOs) to a major component of organic solar cells. We made sandwich-type devices combining a p-type TPCO with fullerene (C_{60}) or an n-type TPCO. As an option we made a device that combined a mixed layer of p-type and n-type TPCOs with the C_{60} layer. All devices indicated rectification properties in the dark and generated electric powers under the white light illumination. The device comprising methoxy-substituted biphenyl-capped bithiophene and C_{60} achieved the best power conversion efficiency of 1.20% with a short-circuit current of 4.28 mA/cm^2 and fill factor of 0.46. The results demonstrate that the TPCO materials are useful as the major component of the organic solar cells.

Keywords Organic photovoltaic cells; thiophene/phenylene co-oligomers; fullerene

Introduction

Light emission and photoelectric conversion are two major optoelectronic properties of semiconductors. Normal solar cells are based upon a p-type semiconductor layer and an n-type semiconductor layer at the interface of which excitons (or excited states) are dissociated into charged carriers (i.e. holes and electrons). This is a basic constitution of the organic solar cells including dye-sensitized solar cells. Within these devices the p-type materials are used for a light absorber where excitons are subsequently generated. Those materials can be chosen from among various materials such as polythiophenes [1], polyphenylenevinylenes [2], phthalocyanines [3, 4], etc. These materials are characterized by high carrier mobility.

In the present studies we have applied thiophene/phenylene co-oligomers (TPCOs) [5-8] to the solar cell materials. Although high emission quantum yield is not necessarily a prerequisite for the solar cell materials, the TPCOs materials are well-known as highly emissive organic semiconductors. Several compounds of them exhibit the laser oscillation in the form of a single crystal [9–12]. This situation is parallel to that for inorganic semiconductors such as gallium arsenide [13, 14]. For sure, the TPCO materials have been applied to solar cell components, but those were used merely for an additional component [15, 16]. In the present studies we have used TPCOs for a major component of a solar cell

*Address correspondence to Shu Hotta, Department of Macromolecular Science and Engineering, Kyoto Institute of Technology, Matsugasaki, Sakyo-ku, Kyoto 606-8585, Japan. Tel.:+81-75-724-7793; Fax:+81-75-724-7800. E-mail: hotta@kit.ac.jp

Color versions of one or more of the figures in the article can be found online at www.tandfonline.com/gmcl.

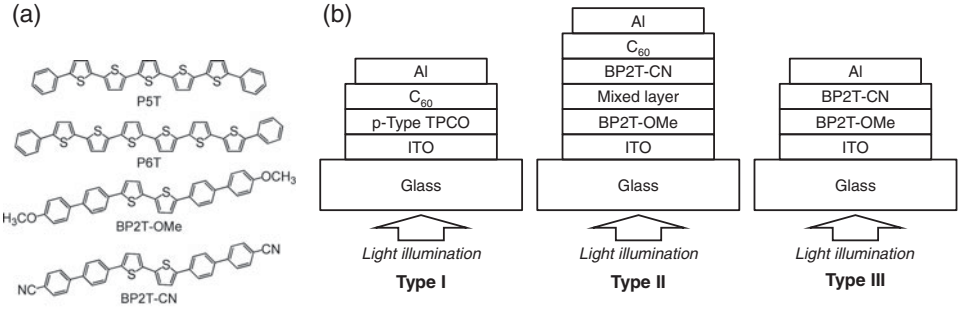

Figure 1. (a) Structural formulae of P5T, P6T, BP2T-OMe, and BP2T-CN. (b) Schematic cross-sections of three types of the solar cells.

and made sandwich-type devices to demonstrate initial results achieved with the TPCOs as novel photovoltaic materials. With the n-type counterpart we used fullerene or another TPCO and the device comprised ITO/p-type TPCO/C_{60} (or n-type TPCO)/Al, where ITO stands for indium tin oxide. As an optional extra we made a device that combined a mixed layer of p-type and n-type TPCOs with the C_{60} layer. The highest power conversion efficiency recorded 1.20%. Details about the experimental results and their implications are presented and discussed.

Experiments

Among TPCOs we used 5,5′′′′-diphenyl-2,2′:5′,2′′:5′′,2′′′:5′′′,2′′′′-quinquethiophene (P5T) [5], 5,5′′′′′-diphenyl-2,2′:5′,2′′:5′′,2′′′:5′′′,2′′′′:5′′′′,2′′′′′-sexithiophene (P6T) [7], 5,5′-bis(4′-methoxybiphenyl-4-yl)-2,2′-bithiophene (BP2T-OMe) [8], and 5,5′-bis(4′-cyanobiphenyl-4-yl)-2,2′-bithiophene (BP2T-CN) [8]. The synthesis and purification methods for the materials are described in the literature [5, 7, 8]. Figure 1(a) shows their structural formulae. P5T, P6T, and BP2T-OMe are p-type materials and BP2T-CN is an n-type material. We purchased C_{60} (98%, 99.5%, and 99.9%) from Sigma-Aldrich Co. LLC. and used them without further purification to form the n-type semiconductor layer.

We fabricated three types of devices. Figure 1(b) shows their schematic cross-sections. For the type I, single-component p-type TPCO and C_{60} layers were sandwiched in between ITO and Al electrodes. For the type II, we replaced the single-component p-type TPCO layer with three-layered TPCOs composed of BP2T-OMe and BP2T-CN. The interlayer was made of a mixed layer of them. For the type III, we sandwiched BP2T-OMe and BP2T-CN layers between electrodes. For all devices we used ITO as a positive electrode and Al as a negative electrode. We formed four isolated thin rectangle ITO electrodes (2 mm × 6.5 mm in size and 150 nm in thickness) on a glass substrate (15 mm × 15 mm) by etching the ITO layer with hydrochloric acid. The substrates were cleaned through ultrasonication in acetone, 2-propanol, ethanol, and distilled water for 10 min each successively and were further treated with UV-ozone for 10 min.

We deposited in vacuum ($\sim 2 \times 10^{-3}$ Pa) the organic materials on the ITO electrodes through a stainless steel mask. The typical deposition rate was 0.01−0.04 nm/s. We summarize in Table 1 the device constitution and fabrication procedures together with the film

Table 1. Constitutions of sandwich-type solar cells. Depositions were carried out from the left to the right. A symbol ↓ indicates the air exposure between the depositions of materials on both sides of it.

		Constitution							
Device	Type	Material (Thickness)							
1	I	ITO (150 nm)	P5T (60 nm)		99.9%-C_{60} (50 nm)			↓	Al (100 nm)
2	I	ITO (150 nm)	P6T (60 nm)	↓	99.5%-C_{60} (100 nm)			↓	Al (100 nm)
3	I	ITO (150 nm)	BP2T-OMe (50 nm)		98%-C_{60} (70 nm)			↓	Al (150 nm)
4	I	ITO (150 nm)	BP2T-OMe (50 nm)	↓	98%-C_{60} (70 nm)			↓	Al (150 nm)
5	II	ITO (150 nm)	BP2T-OMe (20 nm)		Mixed layer (25 nm)	BP2T-CN (7 nm)	99.9%-C_{60} (20 nm)	↓	Al (100 nm)
6	III	ITO (150 nm)	BP2T-OMe (50 nm)		BP2T-CN (70 nm)			↓	Al (100 nm)

thickness of each material. Depositions were carried out from the left to the right with interim air exposure(s), which are marked with a symbol ↓. We termed, e.g., the resulting device with the constitution ITO/P5T/C_{60}/Al Device 1. The mixed layer of Device 5 was formed by co-depositing BP2T-OMe and BP2T-CN in the weight ratio of 1:1 from separate sources such that the total thickness of the mixed layer was 25 nm. We completed the devices by depositing four Al electrodes (2 mm × 7 mm in size) through another stainless steel mask on top of the organic layers in vacuum ($\sim 2 \times 10^{-3}$ Pa) so that the Al electrodes crossed the ITO electrodes. Thus we made four discrete solar cells with a square 2 mm × 2 mm on each glass substrate. The film thicknesses were monitored using a quartz oscillator and determined with an ULVAC DEKTAK-3ST surface profiler.

We measured current-voltage characteristics by using a Keithley 4200-SCS semiconductor parameter analyzer. The devices were mounted in the vacuum chamber and their Al electrodes were grounded. We applied direct-current (DC) voltages of 3.0 to –3.0 V (or 2.0 to –2.0 V for Device I) to the ITO electrodes. The measurements were carried out in vacuum ($\sim 10^{-3}$ Pa) both in the dark and under illumination of white light. The white light was emitted from a mercury lamp (an EXFO X-Cite 120 fluorescence illumination system) via an optical fiber which was placed right above the device at a distance of 119 mm from it. The light was perpendicularly incident on the glass substrate of the device through the glass window of the vacuum chamber [see Fig. 1(b)]. We set the input light intensity at $\sim$100 mW/cm^2.

To perform absorbance and X-ray diffraction (XRD) measurements, we deposited each organic material on a quartz substrate or a silicon substrate covered with a silicon dioxide layer (300 nm in thickness). These were examined using a Shimadzu UV-3600 UV-Vis spectrophotometer and a Rigaku RINT 2500 X-ray diffractometer with Cu Kα radiation.

To evaluate the energy levels and molecular geometry of TPCOs, we carried out density functional theory (DFT) calculation based on the B3LYP method with 6–31G(d) basis set using Gaussian 09 program [17]. The molecular geometry data of P6T and BP2T-OMe were borrowed from the literature [12, 18]. We used the van der Waals radii [19] of hydrogen (1.20 Å) and nitrogen (1.55 Å) to estimate the molecular lengths.

Results and Discussion

Figure 2(a) shows XRD patterns of the organic thin films vacuum-deposited. The peak locations of TPCO films are summarized in Table 2. The BP2T-OMe showed a series of well-defined diffraction lines; the first-order diffraction (the spacing of 28.38 Å) and higher-order diffractions up to the tenth order were clearly resolved. The diffraction spacing is in agreement with a half of the *c*-axis of the crystal (28.16 Å) [12]. These results reflect the presence of the highly aligned structure accompanied by vertical molecular alignment, where the molecular long axis is tilted by a small angle of 17.1° against the normal of the bottom crystal plane (i.e. *ab*-plane) [12]. The P6T film exhibited the first-order diffraction line at 2.74° along with the second- and third-order diffraction lines located at 5.40 and 8.23°, respectively. The plane separation estimated from these lines was 32.21 Å, again in pretty good agreement with the half distance between the adjacent crystal *ab*-planes (30.91 Å) [18]. The diffraction lines at 2.92 and 5.86° of P5T are due to the first- and second-order diffraction lines, respectively. These lines arose from the diffraction spacing of 30.07 Å. This was close to the molecular length of P5T (31.03 Å) calculated by the DFT method. The above XRD data imply that in the vacuum-deposited films of BP2T-OMe, P6T, and P5T a molecular layered structure prevails [20], especially with BP2T-OMe [see Fig. 2(a)]

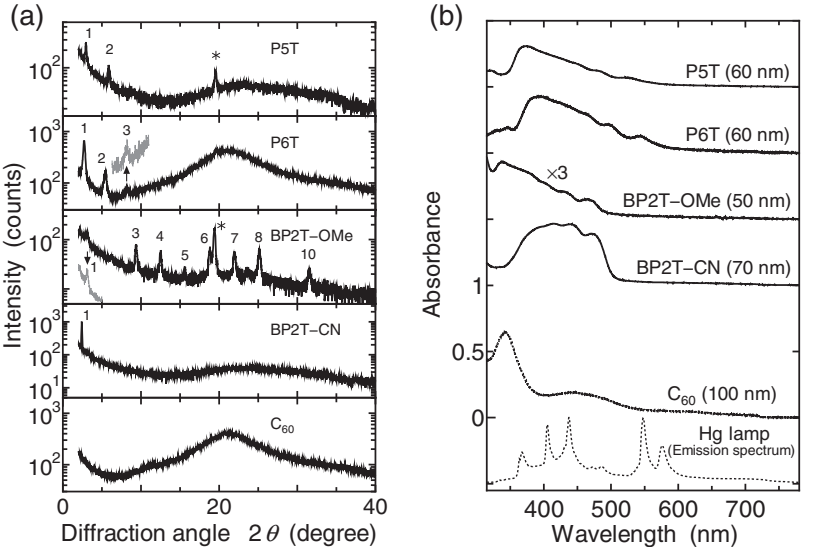

Figure 2. (a) XRD patterns of thin films of TPCOs and C_{60} vacuum-deposited on the quartz or silicon substrates. The raw intensity data were smoothed using a 3-point adjacent average. The numbers represent the first-order and higher-order diffractions with gray curves emphasizing a few of them. The diffractions marked with asterisks denote the lines that were not assigned to the higher-order diffractions. (b) Absorption spectra of the TPCO thin films and the C_{60} thin film. The diagram includes an emission spectrum of the white light from the mercury lamp. The origins are shifted in the longitudinal direction to avoid overlapping. The spectrum of the BP2T-OMe thin film is magnified three times.

[12]. In contrast to the TPCOs, C_{60} indicated no distinct lines within the diffraction angle $2\theta = 2{-}60^\circ$.

Figure 2(b) compares absorption spectra of the thin films of TPCO and C_{60}. The diagram includes the emission spectrum of the mercury lamp. The emissions ranged from 355 to 605 nm. The P5T and P6T films absorbed the light in the wavelength range ∼350−600 nm with their absorption peaking at 374 and 393 nm, respectively. These absorption wavelength ranges overlapped the emission wavelength range of the mercury lamp. The BP2T-OMe film indicated a weak broad absorption around ∼320−500 nm with a maximum at 337 nm. This is consistent with the small tilt of the molecular long axis [12]. The absorption band of BP2T-OMe had no overlap with the emission range of ∼525−605 nm of the mercury lamp. The BP2T-CN film, on the other hand, exhibited a strong absorption around ∼340−510 nm

Table 2. Major peak positions of the XRD patterns for the TPCO thin films.

TPCO	Peak position (°)								
P5T	2.92	5.86	19.56						
P6T	2.74	5.40	8.23						
BP2T-OMe	3.18	9.33	12.52	15.63	18.81	19.37	21.99	25.15	31.54
BP2T-CN	2.41								

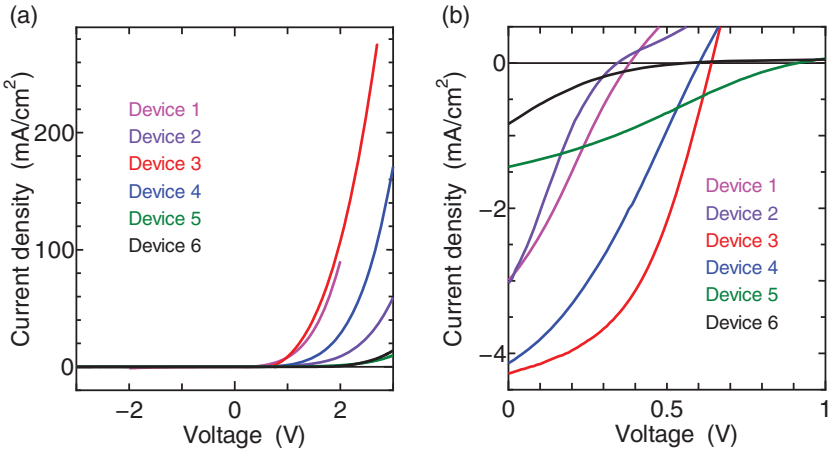

Figure 3. Current-voltage characteristics of the solar cells (a) in the dark and (b) under white light illumination from the mercury lamp. The input light intensity was ∼100 mW/cm^2.

with a maximum at 414 nm. The C_{60} film showed a noticeable maximum at 343 nm together with a broadband around 440 nm.

Figure 3(a) indicates current-voltage characteristics of the solar cells in the dark. All devices show rectification, indicating the p-n junction between the p-type TPCO and n-type C_{60} or BP2T-CN. At the positive voltage, large currents were observed in Devices 1 and 3. Device 3 (the BP2T-OMe/C_{60} device undergoing *no* air exposure in the course of deposition of BP2T-OMe and C_{60}) showed a larger current than Device 4 (the device having the same configuration *with* air exposure). Under the light illumination all devices generated electric powers; see Figure 3(b). Table 3 collects photovoltaic data along with the rectification ratios (calculated at ±2 V). Device 3 achieved the best power conversion efficiency (PCE) of 1.20% with a short-circuit current (J_{SC}) of 4.28 mA/cm^2 and fill factor (FF) of 0.46.

Table 3. Rectification ratio and photovoltaic parameters of the solar cells. P_{in} is the input light intensity. V_{OC} and J_{SC} stand for the open-circuit voltage and the short-circuit current density, respectively. V_{max} and J_{max} correspond to the voltage and current density for the maximum output power, respectively. FF and PCE denote the fill factor and the power conversion efficiency, respectively.

	In the dark	Under illumination						
Device	Rectification ratio (±2 V)	P_{in} (mW/cm^2)	V_{OC} (V)	J_{SC} (mA/cm^2)	V_{max} (V)	J_{max} (mA/cm^2)	FF	PCE (%)
1	69	109	0.38	2.99	0.18	1.69	0.27	0.28
2	510	130	0.35	3.03	0.14	1.56	0.21	0.17
3	26635	105	0.64	4.28	0.41	3.08	0.46	1.20
4	3106	109	0.60	4.13	0.33	2.44	0.32	0.74
5	19	109	0.91	1.44	0.42	0.85	0.27	0.33
6	31	102	0.55	0.84	0.21	0.34	0.15	0.07

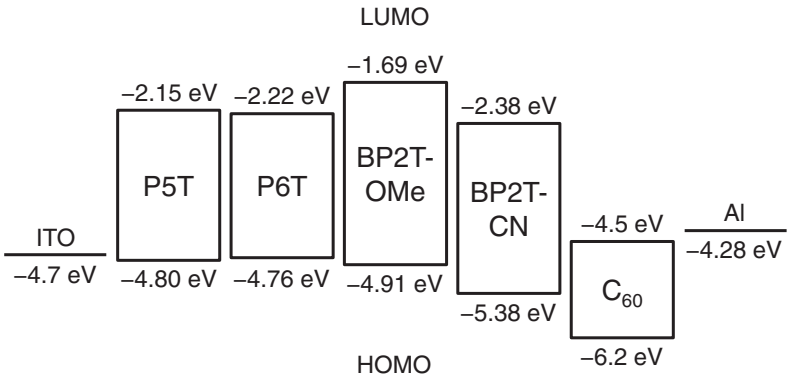

Figure 4. Energy diagrams of TPCOs, C_{60}, ITO, and Al.

This pretty large FF was produced by the convex downward current-voltage characteristics. Even though Device 6 did not include C_{60}, it did indicate a PCE = 0.07% in spite of a small number. The insertion of the BP2T-CN layer also seems to be advantageous to producing a large open-circuit voltage V_{OC} (0.91 V for Device 5; see Table 3) [21].

Figure 4 depicts the highest occupied molecular orbital (HOMO) and lowest unoccupied molecular orbital (LUMO) levels of the organic layers as well as the Fermi levels of ITO [22] and Al [23]. The levels of C_{60} were taken from the literature [24]. It is worth noting that Devices 1−4 exhibited V_{OC} that is systematically larger by up to 0.23 V than a number expected from the band diagram (the difference between HOMO of a TPCO and LUMO of C_{60}) [25]. As an example BP2T-OMe showed V_{OC} of 0.64 V, whereas the expected number was 0.41 V from the diagram (see Figure 4). In this connection Ichikawa et al. [16] determined HOMO and LUMO levels of P6T experimentally. The relevant number of 4.7 eV for the P6T HOMO level was low by 0.2 eV relative to the LUMO of C_{60}, V_{OC} (i.e. 0.35 V) of the P6T-based device (Device 2) again surpassing this difference (Table 3). Note also that the above experimental result is pretty close to the value obtained from the DFT calculation. On this basis we think that more accurate estimation of V_{OC} either theoretical or experimental needs to be done accordingly. The energy differences between the ITO Fermi level and the HOMOs of P5T, P6T, and BP2T-OMe are only 0.10, 0.06, and 0.21 eV, respectively. These small differences facilitate hole transfers from the organic materials to the ITO electrode.

Recently several articles dealt with TPCOs for the purpose of enhancing PCEs. The point is that the TPCO underlayer produces high crystallinity of the photoelectric conversion materials [15, 26]. More specifically, Yu mentioned that the crystalline phthalocyanine layer was formed on top of the BP2T (i.e. one of TPCOs) through "weak epitaxy growth" (WEG) [26]. In light of our experiments we assume that the WEG was caused by the aligned structure of the BP2T layer. Nonetheless, the TPCOs themselves have not used for the photoelectric conversion material [15, 26]. In this respect the present studies clearly demonstrate that the TPCO materials are promising candidates for the photoelectric conversion materials. This approach will be worth pursuing as a new route of organic photovoltaics. A key part of the research is thought to lie in examining extent of exciton diffusion that depends on degree of order (or disorder) of the TPCO layer [27].

We did not carry out the experiments under air mass 1.5 global (AM 1.5 G) illumination from a standard solar simulator [28]. The relevant experiments will have to be conducted

to properly evaluate the performance and activity of TPCOs and compare them with other solar cell materials. Those quantitative investigations remain to be done in the present studies.

Conclusions

We have applied the thin films of TPCOs to a major component of organic solar cells. We fabricated three sandwich-type devices. With the first type, we employed the single-component p-type TPCO layer and the C_{60} layer. As the second type, we replaced the single-component p-type TPCO layer with three layers comprising BP2T-OMe, BP2T-CN, and their mixed interlayer. For the third type device, the BP2T-OMe and BP2T-CN layers were sandwiched between the electrodes.

The XRD patterns of the P5T, P6T, and BP2T-OMe thin films exhibited the first-order and higher-order diffraction peaks, indicating the molecular layered structure in those films. In particular, the BP2T-OMe film indicated the higher-order diffractions up to the tenth order that reflected the highly aligned structure with vertical molecular alignment.

All devices indicated rectification in the dark. Under the white light illumination from a mercury lamp, all devices generated electric powers. Of these, Device 3 achieved the best PCE of 1.20% along with J_{SC} of 4.28 mA/cm^2 and FF of 0.46. The ITO/BP2T-OMe/BP2T-CN/Al device (Device 6) indicated PCE of 0.07%, in spite of the small number. Device 5 showed the larger V_{OC} of 0.91 V in virtue of the insertion of the BP2T-CN layer. Thus, the present studies demonstrate the applicability of the TPCO materials to the major component of the organic solar cells.

Acknowledgments

This work was supported by G8 Research Councils Initiative from Japan Society for the Promotion of Science.

References

[1] Schilinsky, P., Waldauf, C., & Brabec, C. J. (2002). *Appl. Phys. Lett.*, *81*, 3885.
[2] Yu, G., Gao, J., Hummelen, J. C., Wudl, F., & Heeger, A. J. (1995). *Science*, *270*, 1789.
[3] Tang, C. W. (1986). *Appl. Phys. Lett.*, *48*, 183.
[4] Hiramoto, M., Fujiwara, H., & Yokoyama, M. (1992). *J. Appl. Phys.*, *72*, 3781.
[5] Hotta, S., Lee, S. A., & Tamaki, T. (2000). *J. Heterocycl. Chem.*, *37*, 25.
[6] Hotta, S., Kimura, H., Lee, S. A., & Tamaki, T. (2000). *J. Heterocycl. Chem.*, *37*, 281.
[7] Hotta, S., & Katagiri, T. (2003). *J. Heterocycl. Chem.*, *40*, 845.
[8] Katagiri, T., Ota, S., Ohira, T., Yamao, T., & Hotta, S. (2007). *J. Heterocycl. Chem.*, *44*, 853.
[9] Ichikawa, M., Hibino, R., Inoue, M., Haritani, T., Hotta, S., Araki, K., Koyama, T., & Taniguchi, Y. (2005). *Adv. Mater.*, *17*, 2073.
[10] Ichikawa, M., Nakamura, K., Inoue, M., Mishima, H., Haritani, T., Hibino, R., Koyama, T., & Taniguchi, Y. (2005). *Appl. Phys. Lett.*, *87*, 221113.
[11] Yamao, T., Yamamoto, K., Taniguchi, Y., Miki, T., & Hotta, S. (2008). *J. Appl. Phys.*, *103*, 093115.
[12] Mizuno, H., Haku, U., Marutani, Y., Ishizumi, A., Yanagi, H., Sasaki, F., & Hotta, S. (2012). *Adv. Mater.*, *24*, 5744.
[13] Loferski, J. J. (1956). *J. Appl. Phys.*, *27*, 777.
[14] Hall, R. N., Fenner, G. E., Kingsley, J. D., Soltys, T. J., & Carlson, R. O. (1962). *Phys. Rev. Lett.*, *9*, 366.
[15] Chen, W., Qiao, X., Yang, J., Yu, B., & Yan, D. (2012). *Appl. Phys. Lett.*, *100*, 133302.

[16] Ichikawa, M., Suto, E., Jeon, H.-G., & Taniguchi, Y. (2010). *Org. Electron.*, *11*, 700.
[17] Gaussian 09 Revision B.01 (Gaussian, Inc., Wallingford, CT, 2009).
[18] Hotta, S., Goto, M., Azumi, R., Inoue, M., Ichikawa, M., & Taniguchi, Y. (2004). *Chem. Mater.*, *16*, 237.
[19] Bondi, A. (1964). *J. Phys. Chem.*, *68*, 441.
[20] Hotta, S., Ichino, Y., Yoshida, Y., & Yoshida, M. (2000). *J. Phys. Chem. B*, *104*, 10316.
[21] Mutolo, K. L., Mayo, E. I., Rand, B. P., Forrest, S. R., & Thompson, M. E. (2006). *J. Am. Chem. Soc.*, *128*, 8108.
[22] Adachi, C., Baldo, M. A., Thompson, M. E., & Forrest, S. R. (2001). *J. Appl. Phys.*, *90*, 5048.
[23] Michaelson, H. B. (1977). *J. Appl. Phys.*, *48*, 4729.
[24] Peumans, P., & Forrest, S. R. (2001). *Appl. Phys. Lett.*, *79*, 126.
[25] Hiramoto, M. (2012). *Mol. Sci.*, *6*, A0052.
[26] Yu, B., Huang, L., Wang, H., & Yan, D. (2010). *Adv. Mater.*, *22*, 1017.
[27] Najafov, H., Lee, B., Zhou, Q., Feldman, L. C., & Podzorov, V. (2010). *Nat. Mater.*, *9*, 938.
[28] Katz, E. A., Faiman, D., Tuladhar, S. M., Kroon, J. M., Wienk, M. M., Fromherz, T., Padinger, F., Brabec, C. J., & Sariciftci, N. S. (2001). *J. Appl. Phys.*, *90*, 5343.